Journal of Materials Chemistry A

Fast Na-Diffusive Tin Alloy for All-Solid-State Na-Based Batteries

Journal:	*Journal of Materials Chemistry A*
Manuscript ID	TA-COM-05-2023-002787.R2
Article Type:	Communication
Date Submitted by the Author:	11-Nov-2023
Complete List of Authors:	Tanibata, Naoto; Nagoya Institute of Technology, Advanced Ceramics Matsunoshita, Koki; Nagoya Institute of Technology Takeuchi, Hirokazu; Nagoya Institute of Technology Akatsuka, Suzuno; Nagoya Institute of Technology Koga, Misato; Nagoya Institute of Technology Takeda, Hayami; Nagoya Institute of Technology Creative Engineering Program, Nakayama, Masanobu; Nagoya Institute of Technology, Department of Materials Science and Engineering

ARTICLE

Fast Na-Diffusive Tin Alloy for All-Solid-State Na-Based Batteries

Naoto Tanibata*[a], Koki Matsunoshita[a], Hirokazu Takeuchi[a], Suzuno Akatsuka[a], Misato Koga[a], Hayami Takeda[a] and Masanobu Nakayama[a]

Received 00th January 20xx,
Accepted 00th January 20xx

DOI: 10.1039/x0xx00000x

All-solid-state Na batteries, which are inexpensive and highly stable, are promising candidates for energy storage in environmentally friendly microgrids and vehicles. Na diffusivity is an important parameter for the performance of these batteries. In this study, we found that the metastable phase $Na_{10}Sn_4$ exhibits fast Na diffusivity (room temperature diffusion coefficient D_{25} = 5.4×10^{-7} cm^2 s^{-1}), surpassing that of other reported alloys (Sb- and Ge- alloys) as well as oxide and sulfide materials. $Na_{10}Sn_4$ was synthesised by a mechanochemical method, and its electrode properties were evaluated for an all-solid-state battery. The cell exhibited an interfacial resistance of 100.1 Ω cm^2, which is smaller than those reported between metallic anodes and solid or liquid electrolytes. These results indicate that $Na_{10}Sn_4$ has significant potential as an ultra-low-resistance electrode to improve all-solid-state Na batteries, which is a major step forward in energy storage materials research.

Introduction

Recently, the demand for electricity grids and the use of electric vehicles and other electric devices have increased. In this context, the burden on electricity grids must be reduced. Microgrids allow for the local storage of electricity using rechargeable batteries; hence, their construction plays an important role in solving this problem.[1] All-solid-state Na-based batteries, which have a high energy density and are leakage-free and safe, are expected to play a role in this venture because they are inexpensive.[2] In Na-based batteries, wherein Na is exchanged between electrodes, the mobility of Na is one of the most important parameters.[3] Therefore, electrolyte and electrode materials that allow fast Na diffusion through solids have been widely studied to improve battery performance.[4] In this study, we report a metastable phase of a Na–Sn alloy, $Na_{10}Sn_4$, which exhibits fast Na diffusivity (diffusion coefficient D_{25} = 5.4 × 10^{-7} cm^2 s^{-1}) at room temperature.

Na–Sn alloys (e.g., $Na_{15}Sn_4$) are often used as counter electrodes to evaluate the performance of working electrodes in all-solid-state Na secondary batteries.[5] Such counter electrodes require low resistance, necessitating high Na diffusivity, high electronic conductivity, fast charge transfer at the electrode–electrolyte interface, and high cycle stability.[6] Na metal is generally used for such counter electrodes in conventional liquid batteries.[7] However, it is worth noting that active Na metal electrodes often degrade the sulphide solid electrolytes (e.g. Na_3PS_4)[8] found in all-solid-state batteries.[9] Material degradation complicates electrochemical measurements and is a major barrier in battery material research.[10] Alloying with Sn metal is preferred because a Na–Sn alloy system chemically stabilises the interface between the anode and solid electrolyte.[11] In this study, we focused on the metastable phase $Na_{10}Sn_4$, identified only in the initial Na absorption process on a thin Sn film, as the low-resistance counter electrode.[12] The phase has the space group *R*-3*m*, as determined using the cluster expansion method describing the total energy in terms of the configurational degrees of freedom.[12] The metastable phase, which was expected to have high diffusivity,[13] was synthesised via a mechanochemical method useful for metastable phase stabilisation,[14] and its resistance characteristics in all-solid-state batteries were evaluated to identify stable and low-energy-loss electrode materials.

Results and discussion

Figure 1 shows the XRD patterns of the prepared Na–Sn alloys. All Bragg peaks are consistent with the simulated patterns of the $Na_{10}Sn_4$ and $Na_{15}Sn_4$ crystal structures, and no impurity peaks are observed. $Na_{10}Sn_4$ is a metastable phase[12] obtained at room temperature via mechanochemical synthesis. DTA and XRD measurements were performed to investigate the thermal stability of the $Na_{10}Sn_4$ phase (Figure S1). The results show that no endothermic and exothermic peaks were observed in the DTA curve up to 400 °C, and the $Na_{10}Sn_4$ phase was maintained in the XRD pattern after the DTA measurement.

Figure S2 shows SEM images of the powder and fractured surface of the $Na_{10}Sn_4$ electrode. $Na_{10}Sn_4$ electrode powder with a grain size of several micrometres was compacted to form a dense body with necking between the particles. These $Na_{10}Sn_4$ and $Na_{15}Sn_4$ electrodes were evaluated using the Na_3PS_4 solid electrolyte most commonly used in all-solid-state Na-ion batteries.[8] Figure 2 shows the results of constant-current

[a] Department of Advanced Ceramics Institution Nagoya Institute of Technology, Gokiso, Showa, Nagoya, Aichi 466-8555, Japan
* tanibata.naoto@nitech.ac.jp

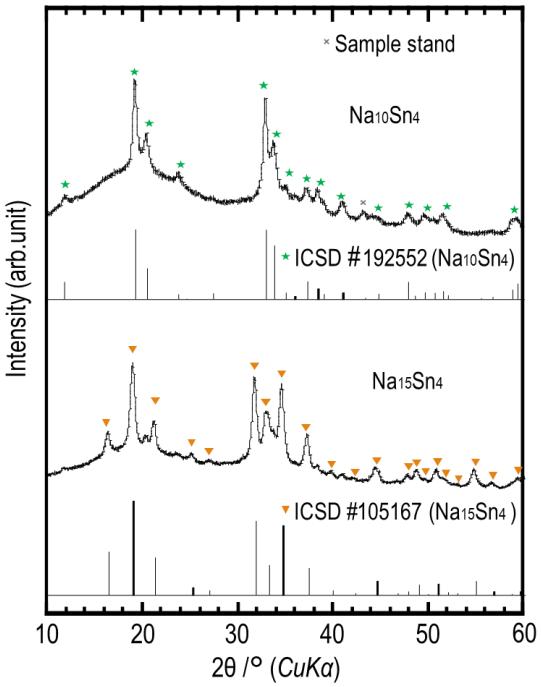

Figure 1. XRD patterns and ICSD data for the $Na_{10}Sn_4$ and $Na_{15}Sn_4$ samples after ball milling. An airtight sample stand was used for the measurements in an Ar atmosphere.

cycling tests at room temperature for the $Na_{10}Sn_4$ | Na_3PS_4 | $Na_{10}Sn_4$, Na | Na_3PS_4 | Na, and $Na_{15}Sn_4$ | Na_3PS_4 | $Na_{15}Sn_4$ symmetric cells; $Na_{10}Sn_4$ exhibits the lowest overvoltage. Note that under the operating conditions of the all-solid-state Na^+ battery, there were no signs of dendrite growth that would lead to a short-circuit condition with a resistance of 0 Ω. The XRD patterns of the Na electrode after charge–discharge are shown in Figure S3. In addition to peaks of the Na electrode and Na_3PS_4 solid electrolyte, peaks of Na_2S are present, indicating that the Na metal degraded the Na_3PS_4. Conversely, no significant change is observed in the XRD pattern of the Na–Sn alloy electrode before and after charge–discharge (Figure S4). This indicates that the Sn alloying successfully suppressed the reactivity of the Na metal. Furthermore, although $Na_{10}Sn_4$ is a metastable phase, the crystalline structure was retained after charge–discharge. In addition, as shown in Figure S5, $Na_{10}Sn_4$ shows a stable charge–discharge performance and crystal structure even at 100 °C, which is above the melting point of Na (98 °C). Evaluation at such high temperatures is difficult with conventional cells using organic electrolytes because of their thermal instability above 50 °C;[15] therefore, all-solid-state batteries using $Na_{10}Sn_4$ can expand the evaluation temperature range of the electrode material. Figure S6 shows the results of long cycling tests at room temperature with a current density of 0.1 mA cm^{-2}; $Na_{10}Sn_4$ exhibits a stable, low overvoltage over 100 cycles.

The overvoltages for the symmetric cell with $Na_{15}Sn_4$ electrodes are smaller than those of the Na electrodes but slightly larger than those of $Na_{10}Sn_4$ (Figure 2 (c)). AC impedance measurements were also obtained to analyse the overvoltages. The $Na_{10}Sn_4$ symmetric cell shows the lowest and most stable resistance (Figure 2 (d)–(f)), which is consistent with the charge–discharge curve results. Resistance of the Na electrode increases with each cycle, indicating that it is unsuitable as a counter electrode with the Na_3PS_4 electrolyte. The $Na_{15}Sn_4$ symmetric cell does not show a clear increase in resistance similar to that of the Na metal; however, it exhibits a larger resistance than the $Na_{10}Sn_4$ symmetric cell. Resistance separation was performed in the cells after cycling to clarify these results. The observed semi-circles in these impedance plots may include the electrode/electrolyte interface resistance and the electrolyte layer resistance. Therefore, the electrode/electrolyte interface resistance was calculated by subtracting the resistance of the electrolyte-only cell (565 Ω, Figure S7) from the semi-circle resistance after the last charge–discharge cycle. The resistance was normalised by the area per electrode and per pellet (0.785 cm^2). Table 1 compares the calculated interfacial resistances with those of other representative Na battery systems. The interface resistance (100.1 Ω cm^2) of the $Na_{10}Sn_4$ electrode is lower than that of the system with Na and $Na_{15}Sn_4$ electrodes[16] and the system with an electrolyte solution,[17] whereas it is comparable to that of the oxide systems in practical use (191 Ω cm^2 for Na | β''-alumina, etc.).[18] The low interfacial resistance of $Na_{10}Sn_4$ may be because of the stabilising effects of the Sn component on Na, which also gives a larger and more stable reduction potential (~0.13 V vs Na/Na^+) than that of $Na_{15}Sn_4$ (~0.11 V vs Na/Na^+) discussed below. However, further detailed interfacial structure analysis is required to confirm this hypothesis.

Table 1. Interfacial resistance of metal anode | electrolyte in representative Na-based batteries.

Interface of metal anode | electrolyte	Area-specific resistance [Ω cm^2]	Reference No.
$Na_{10}Sn_4$ | Na_3PS_4	**100.1**	**This study**
$Na_{15}Sn_4$ | Na_3PS_4	**477.8**	**This study**
Na | Na_3PS_4	**14860**	**This study**
Na | Na_3PS_4	3740	16
Na | $Na_{2.94}PS_{3.94}Cl_{0.0625}$	2139	16
Na | NASICON ($Na_{3.2}Zr_{1.90}Mg_{0.10}Si_2PO_{12}$)	1658	19
Na | Na-β''-Al_2O_3	191	18
Na | Typical liquid electrolyte ($NaPF_6$-soluted EC-DMC liquid)	700	17

Next, to quantitatively compare the Na diffusion coefficients within the Sn alloys, the Warburg coefficient, A_w,[20] was calculated for each system from the linear portion of the AC impedance at low frequencies (Figure S8). The Warburg coefficient for $Na_{10}Sn_4$ (22.3 Ω $s^{1/2}$) was lower than that of $Na_{15}Sn_4$ (37.8 Ω $s^{1/2}$), indicating higher Na diffusivity in the $Na_{10}Sn_4$ electrode. The Warburg coefficient of $Na_{10}Sn_4$ after the discharge process (20.0 Ω $s^{1/2}$) calculated from Figure S9 indicated that the diffusivity did not vary significantly with alloy composition. To obtain the diffusion coefficient (generally used as a measure of the diffusivity of a material) from the Warburg coefficient, the slope, *b*, of the OCV is required, as determined by the following equation:

$$D = \left(\frac{b v_m}{\sqrt{2} F S A_w}\right)^2, \quad (1)$$

where v_m is the molar volume of the active material, *S* is the electrode reaction area, *D* is the diffusion coefficient, and *F* is Faraday's constant. However, in a symmetric cell, calculating an accurate value for the slope of OCV is difficult because both electrodes contribute to the reaction. Therefore, a cell with a Na counter electrode, whose OCV does not change with charge–discharge, was fabricated, and the diffusion coefficient was evaluated. Note that the degradation of Na, as seen in Figure 2 (e), results in an underestimation of the calculated diffusion coefficient. To minimise this effect, the constant-current pulse method,[21] which provides a signal in a shorter time than AC impedance, was employed. Constant-voltage pulse measurements are also used similarly. However, this time the constant-current pulse method was chosen because the influence of interference of resistance polarisations (e.g. ohmic and charge-transfer resistances) can be eliminated as long as these polarisations are fixed.[22] In the constant-current pulse method, the diffusion coefficient is calculated using the following equations:[31]

$$D = \frac{4}{\pi}\left(\frac{b I v_m}{F S}\right)^2 \left(\frac{\sqrt{t}}{\Delta E}\right)^2, \quad (2)$$

$$\Delta E = E - (E_0 + IR), \quad (3)$$

where E_0 is the voltage before current application, *IR* is the voltage that instantaneously changes by Ohm's law, Δ*E* is the voltage change in the curved region, *I* is the applied current, v_m is the molar volume of the active material, *b* is the slope of OCV, *t* is the current application time, *F* is Faraday's constant, *S* is the electrode reaction area, and *D* is the diffusion coefficient.

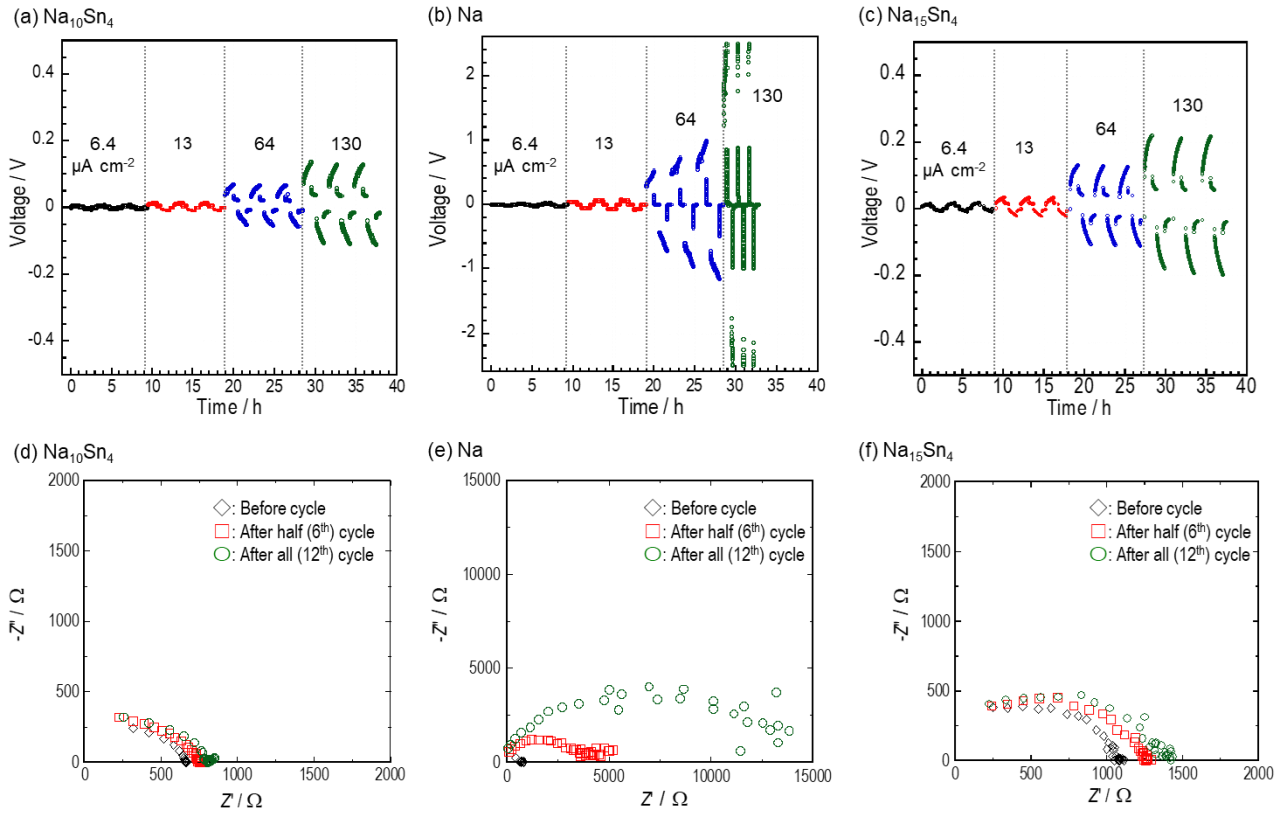

Figure 2. Evaluation of the $Na_{10}Sn_4$, Na, and $Na_{15}Sn_4$ electrodes in the all-solid-state Na batteries using Na_3PS_4 sulphide electrolyte. Constant-current cycling test results of (a) $Na_{10}Sn_4$, (b) Na, and (c) $Na_{15}Sn_4$ symmetric cells. The numbers in the graphs indicate the current density (μA cm^{-2}). AC impedance plots of (d) $Na_{10}Sn_4$, (e) Na, and (f) $Na_{15}Sn_4$ symmetric cells. The data shown was collected before, halfway through, and after the constant-current cycling test.

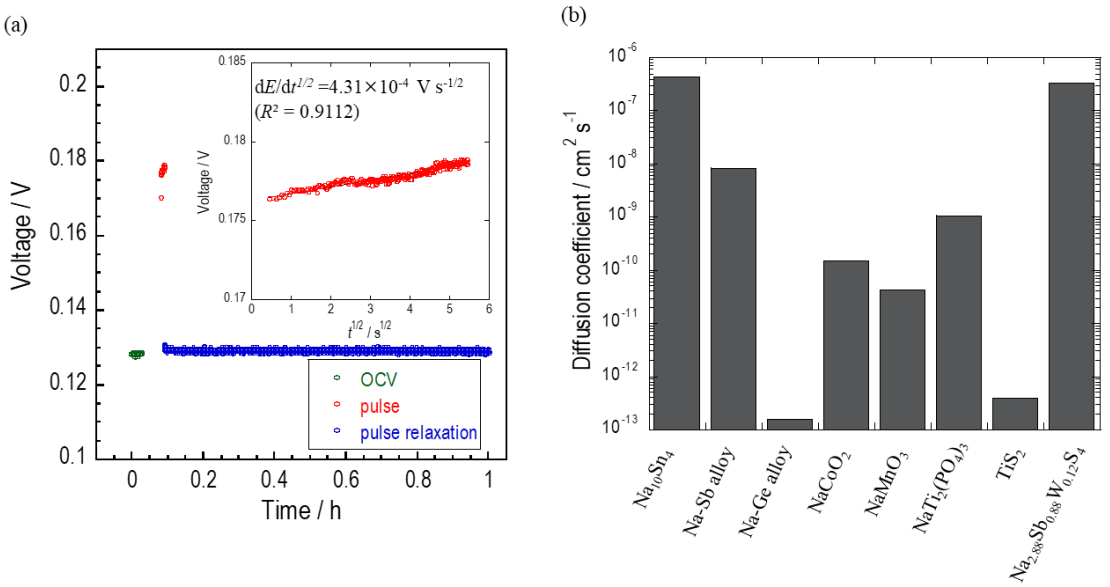

Figure 3. Diffusivity evaluation of $Na_{10}Sn_4$. (a) Constant-current pulse measurements in a Na/$Na_{10}Sn_4$ cell; the inset shows the voltage variation versus the square root of time during the current pulse application. The diffusion coefficient is calculated from the slope. (b) Comparison of Na diffusion coefficients for Na battery materials. The diffusion coefficients used for comparison are the maximum values in the charge–discharge process evaluated for thin film. The $Na_{2.88}Sb_{0.88}W_{0.12}S_4$ diffusion coefficient is the conductivity diffusion coefficient calculated from the Nernst–Einstein formula.

Figure 3 (a) shows the results of the constant-current pulse measurement. The inset plots the voltage change, Δ*E*, versus the square root of time, $\sqrt{t}$, during the current pulse portion. The diffusion coefficient is calculated from the slope of this line using Equation (2). Herein, the slope of the OCV, *b*, is the change in voltage versus the solid-solution reaction rate. Therefore, constant-current charge–discharge measurements were also performed (Figure S10) to investigate the capacity of this electrode for the solid-solution reaction. During charging, Na desorption is observed in $Na_{10-x}Sn_4$ with an x of approximately 7, indicating reversible discharge with a capacity of 264 mAh g^{-1} in the first cycle. This cell showed similar behaviour in the second cycle. The charge–discharge behaviour is different from that of a previously reported Na–Sn alloy[23] where all Na is desorbed from Sn upon a charge cut-off potential of 1 V (vs. Na/Na^+), indicating that the $Na_{10}Sn_4$ electrode is an attractive candidate for further research owing to its unique metastable reaction. In addition, the relatively high capacity and low potential indicate that this material may also be promising as a full-cell type anode material. Such applications and the charge–discharge mechanism should be investigated in the future. A single slope is observed from the beginning of the charge up to x of approximately 3.6 in $Na_{10-x}Sn_4$. From the Wykoff positions of $Na_{10}Sn_4$ (space group: *R*-3*m*) shown in Table S1, four Na atoms in $Na_{10}Sn_4$ are distributed to one 6c site, four to another 6c site, and the remainder to two 3b sites. In addition, an energy comparison of the post-defect structures of each Na site shown in Table S2 also suggests that one of the 6c sites is also the most thermodynamically unstable. Therefore, the slope with the capacity of x ≈ 3.6 corresponds to a solid-solution reaction of the four Na atoms desorption at one of the 6*c* sites. The capacity of the current pulse in Figure 3 (a) was converted to the solid-solution reaction rate using this value, and the slope of the OCV (*b* = 1.86 V) was calculated from the change in OCV before and after the pulse. The value of OCV after this relaxation (0.13 V vs Na/Na^+) was taken as the potential of $Na_{10}Sn_4$ relative to Na. The slope of the change in voltage with respect to the square root of time ($dE/dt^{1/2}$) during the application of the current pulse is 4.31×10^{-4} V $s^{-1/2}$ (Figure 3(a)). The electrode/electrolyte interface (*S*) area was set as the area of the 10 mmϕ-diameter measurement cylinder (*S* = 0.785 cm^2). This accounts for the spreading of the 6 mmϕ Na foil during pressing, thereby avoiding the overestimation of the diffusion coefficient. Nevertheless, the calculated diffusion coefficient, *D*, is 5.4×10^{-7} cm^2 s^{-1}. As compared in Figure 3 (b), this diffusion coefficient is higher than that of the other alloy materials ($Na_{3-x}Sb$[24] 1.3×10^{-10}–8.5×10^{-9} cm^2 s^{-1} and Na_xGe[25] 9.0×10^{-14}–1.6×10^{-13} cm^2 s^{-1}) and the oxide and sulphide electrode materials (Na_xCoO_2[26] 0.5–1.5×10^{-10} cm^2 s^{-1}, Na_xMnO_3[27] 0.8–4.3×10^{-11} cm^2 s^{-1}, $NaTi_2(PO_4)_3$[28] 2.4×10^{-12}–1.0×10^{-9} cm^2 s^{-1}, and TiS_2[29] 7.3×10^{-17}–3.9×10^{-13} cm^2 s^{-1}). Note that these comparisons were evaluated for bulk materials, such as thin films, to compare only material properties, and the maximum values during charging and discharging were used. The diffusion coefficient of $Na_{10}Sn_4$ in this study was found to be higher than that recently reported (3.3×10^{-7} cm^2 s^{-1}) for a super-Na ionic conductor $Na_{2.88}Sb_{0.88}W_{0.12}S_4$ (ionic conductivity = 3.2×10^2 S cm^{-1}).[30] Ionic conductivity was calculated by the Nernst–Einstein equation as follows:

$$\sigma = \frac{z^2 F^2 cD}{RT}, \qquad (4)$$

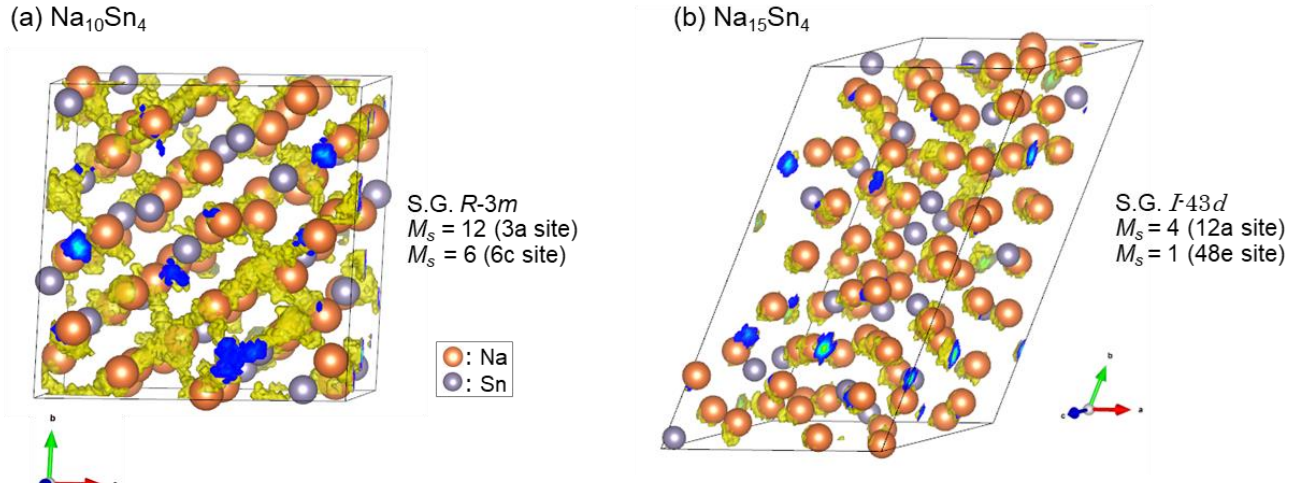

Figure 4. Probability density distribution of Na in DFT–MD calculation for (a) $Na_{10}Sn_4$ and (b) $Na_{15}Sn_4$ at temperature 25 ˚C. Site symmetry, M_s, is expressed as the multiplicity of general position divided by site multiplicity.

where *z* is the valence of the ion, *F* is the Faraday constant, *c* is the concentration of the carrier ion, *R* is the gas constant, *T* is the temperature, and σ is the ionic conductivity. The ionic conductivity of $Na_{10}Sn_4$ calculated by the Nernst–Einstein equation is 6.1 × 10^{-2} S cm^{-1}. This high sodium diffusivity, in addition to the low interface resistance between the electrode/electrolyte mentioned earlier, contributes to the excellent charge–discharge characteristics of $Na_{10}Sn_4$.

To investigate the cause of the fast Na diffusivity in $Na_{10}Sn_4$, we performed a first-principles molecular dynamics (MD) simulation analysis. Figure S11 shows the mean squared displacement (MSD) calculated as follows:

$$MSD(t) = \frac{1}{nm}\sum_{i}^{n}\sum_{k}^{m}|r_i(t_k + t) - r_i(t_k)|^2, \quad (5)$$

where *n* is the number of atoms, *m* is the number of time series data, *r* is the distance travelled by *i* atoms, and t_k is the start time of the k^{th} time series data. In both $Na_{10}Sn_4$ and $Na_{15}Sn_4$, only Na diffuses with increasing time. From the slope of the MSD of Na, the diffusion coefficient D was calculated using the following equation:

$$MSD = 2dDt\,, \quad (6)$$

where *d* is the diffusion dimension (here, d = 3). The results show that $Na_{10}Sn_4$ has a higher diffusion coefficient (1.2 × 10^{-6} cm^2 s^{-1}) than that of $Na_{15}Sn_4$ (1.4 × 10^{-10} cm^2 s^{-1}), similar to the experimental results. The diffusion coefficient of $Na_{10}Sn_4$ is also higher than that of other alloys calculated by first-principles MD calculations (NaSi: 8.31 × 10^{-9} cm^2 s^{-1}, NaGe: 2.87 × 10^{-8} cm^2 s^{-1}, and NaSn: 3.66 × 10^{-8} cm^2 s^{-1}).[31] The trajectories of Na in each MD for $Na_{10}Sn_4$ and $Na_{15}Sn_4$ are shown in Figure 4. While only localised diffusion is observed for $Na_{15}Sn_4$, a clear 3D diffusion path is observed for $Na_{10}Sn_4$. Since metastable phases tend to have good symmetry,[32] this highly symmetric 3D conduction pathway may be attributed to $Na_{10}Sn_4$ being a metastable phase.[12] Moreover, highly symmetrical structures often have low diffusion activation energies.[13]

To demonstrate the high symmetry of $Na_{10}Sn_4$, the symmetry of the carrier Na site was defined as M_s = general position multiplicity m_g/site multiplicity m_s" and compared with the stable phase, $Na_{15}Sn_4$. $Na_{10}Sn_4$ (*R*-3*m*, m_g of general position: 36) has M_s = 12 at site 3a and M_s = 6 at site 6c, which is larger than the M_s (4 at site 12a and 1 at site 48e) of $Na_{15}Sn_4$ (*I*-43*d*, m_g of general position: 48). This indicates that the metastable phase $Na_{10}Sn_4$ has a higher symmetry, which may contribute to its high diffusivity. In addition, $Na_{10}Sn_4$ is an alloy and, therefore, has more metallic bonding than other oxide and sulphide materials. Because metallic bonding involves free electrons, the anisotropy of the bonding is smaller than that of ionic or covalent bonding, which may reduce the Na diffusion activation energy. Further investigation of the source of the high Na diffusivity of this binary alloy is planned. Finally, the charge–discharge cycle characteristics of the full cells with a TiS_2 cathode (Figure S12) indicate that changing the anode from $Na_{15}Sn_4$ to $Na_{10}Sn_4$ improves the initial capacity and capacity retention of the cell.

Conclusions

The metastable phase $Na_{10}Sn_4$ was characterised as a low-resistance counter electrode in all-solid-state Na-ion batteries. The $Na_{10}Sn_4$ electrode showed a stable, small interfacial resistance and high Na diffusivity. This $Na_{10}Sn_4$ electrode exhibited a higher room temperature diffusion coefficient (5.4 × 10^{-7} cm^2 s^{-1}) than other alloys and oxide and sulphide materials. Na diffusivity is an important parameter in Na-based batteries, and this research has led to the discovery of a material with ideal properties. This low-resistance counter electrode may enable significant research on the properties of electrode materials for environmentally friendly, high-energy-storage, all-solid-state Na^+ batteries, including the $Na_{10}Sn_4$ alloy itself. This material is a well-studied binary system, and it

highlights the importance and potential of metastable phases in the material research space.

Author Contributions

N. T. and M. N. conceived and designed the experiments; K. M. and S. A. performed the experiments and analysed the data; H. T. and H. T. contributed calculations and materials/analysis tools; N. T. and M. N. co-wrote the paper. N. T. is the corresponding author (e-mail: tanibata.naoto@nitech.ac.jp).

Conflicts of interest

There are no conflicts to declare.

Acknowledgements

This work was supported in part by the 'Advanced Low Carbon Technology Research and Development Program' of the Japan Science and Technology Agency (JST), Japan (since 2013); Grant-in-Aid for Scientific Research (grant numbers 19H05815, 19K15657, 20H02436, 21K14715, 21H01625, and 22H02179); Ministry of Education Culture, Sports, Science and Technology, Japan (MEXT), 'Data creation/utilisation type material research and development project' (grant number, JPMXP1122712807); MEXT, Program for Promoting Research on the Supercomputer Fugaku (Fugaku Battery & Fuel Cell Project, grant number JPMXP1020200301); and CREST of JST (grant numbers JPMJCR21O6 and JPMJCR21D3). We also thank the Information Technology Centre of Nagoya University for providing computing resources (CX400).

Notes and references

1 B. Dunn, H. Kamath and J.-M. Tarascon, *Science*, 2011, **334**, 928.
2 L. Shen, J. Yang, G. Liu, M. Avdeev and X. Yao, *Mater. Today Energy*, 2021, **20**, 100691.
3 N. Yabuuchi, K. Kubota, M. Dahbi and S. Komaba, *Chem. Rev.*, 2014, **114**, 11636.
4 C. Delmas, Adv. *Energy Mater.*, 2018, **8**, 1703137.
5 F. Hao, X. Chi, Y. Liang, Y. Zhang, R. Xu, H. Guo, T. Terlier, H. Dong, K. Zhao, J. Lou and Y. Yao, *Joule*, 2019, **3**, 1349.
6 A.L. Santhosha, L. Medenbach, J.R. Buchheim and P. Adelhelm, *Batter. Supercaps.*, 2019, **2**, 524.
7 K. Chayambuka, G. Mulder, D.L. Danilov and P.H.L Notten, *Adv. Energy Mater.*, 2018, **8**, 1800079.
8 A. Hayashi, K. Noi, A. Sakuda and M. Tatsumisago, *Nat. Commun.*, 2012, **3**, 856.
9 Y. Tian, Y. Sun, D.C. Hannah, Y. Xiao, H. Liu, K.W. Chapman, S.H. Bo and G. Ceder, *Joule*, 2019, **3**, 1037.
10 D.H.S. Tan, A. Banerjee, Z. Chen and Y.S. Meng, *Nat. Nanotechnol.*, 2020, **15**, 170.
11 J.A.S. Oh, J. Sun, M. Goh, B. Chua, K. Zeng and L. Lu, *Adv. Energy Mater.*, 2021, **11**, 2101228.
12 L. Baggetto, P. Ganesh, R.P. Meisner, R.R. Unocic, J.-C.C. Jumas, C.A. Bridges and G.M. Veith, *J. Power Sources*, 2013, **234**, 48.
13 M.C. Verbraeken, C. Cheung, E. Suard and J.T.S. Irvine, *Nat. Mater.*, 2015, **14**, 95.
14 A.F. Fuentes, L. Takacs, *J. Mater. Sci.*, 2012, **48**, 598.
15 A. Ponrouch, D. Monti, A. Boschin, B. Steen, P. Johansson and M.R. Palacín, *J. Mater. Chem. A*, 2014, **3**, 22.
16 E.A. Wu, C.S. Kompella, Z. Zhu, J.Z. Lee, S.C. Lee, I.H. Chu, H. Nguyen, S.P. Ong, A. Banerjee and Y.S. Meng, *ACS Appl. Mater. Interfaces*, 2018, **10**, 10076.
17 D.I. Iermakova, R. Dugas, M.R. Palacín and A. Ponrouch, *J. Electrochem. Soc.*, 2015, **162**, A7060.
18 S. Wenzel, T. Leichtweiss, D.A. Weber, J. Sann, W.G. Zeier and J. Janek, *ACS Appl. Mater. Interfaces*, 2016, **8**, 28216.
19 H. Fu, Q. Yin, Y. Huang, H. Sun, Y. Chen, R. Zhang, Q. Yu, L. Gu, J. Duan and W. Luo, *ACS Mater. Lett.*, 2020, **2**, 127.
20 P. Zhan, S. Wang, Y. Yuan, K. Jiao and S. Jiao, *J. Electrochem. Soc.*, 2015, **162**, A1028.
21 D. Zehnder, C. Deshpandey, B. Dunn and R.F. Bunshah, *Solid State Ion.*, 1986, **18–19**, 813.
22 L.D. Ellis, T.D. Hatchard and M.N. Obrovac, *J. Electrochem. Soc.*, 2012, **159**, A1801.
23 L. Baggetto, P. Ganesh, C.N. Sun, R.A. Meisner, T.A. Zawodzinski and G.M. Veith, *J. Mater. Chem. A*, 2013, **1**, 7985.
24 P.R. Abel, Y.M. Lin, T. De Souza, C.Y. Chou, A. Gupta, J.B. Goodenough, G.S. Hwang, A. Heller and C.B. Mullins, *J. Phys. Chem. C*, 2013, **117**, 18885.
25 T. Shibata, Y. Fukuzumi, W. Kobayashi and Y. Moritomo, *Sci. Rep.*, 2015, **5**, 1.
26 Y. Xu, M. Zhou, X. Wang, C. Wang, L. Liang, F. Grote, M. Wu, Y. Mi and Y. Lei, Angew. *Chem. Int. Ed.*, 2015, **54**, 8768.
27 F. Sagane, *J. Electrochem. Soc.*, 2016, **163**, A2835.
28 F.N. Sayed, M.B. Sreedhara, A. Soni, U. Bhat, R. Datta, A.J. Bhattacharyya and C.N.R. Rao, *Mater. Res. Express*, 2019, **6**.
29 A. Hayashi, N. Masuzawa, S. Yubuchi, F. Tsuji, C. Hotehama, A. Sakuda and M. Tatsumisago, *Nat. Commun.*, 2019, **10**, 1.
30 C.Y. Chou, M. Lee, G.S. Hwang, *J. Phys. Chem. C*, 2015, **119**, 14843.
31 J.L.F. Da Silva, A. Walsh and H. Lee, *Phys. Rev. B Condens. Matter Mater. Phys.*, 2008, **78**, 224111.